JAAS

ROYAL SOCIETY OF CHEMISTRY

PAPER

View Article Online
View Journal | View Issue

Cite this: *J. Anal. At. Spectrom.*, 2024, **39**, 227

Strategies to enhance figures of merit in ICP-ToF-MS

T. E. Lockwood, [a] R. Gonzalez de Vega, [b] Z. Du,[c] L. Schlatt,[d] X. Xu [c] and D. Clases *[b]

Inductively coupled plasma with time-of-flight mass spectrometry (ICP-ToF-MS) is currently setting new benchmarks for the analysis of single particles (SP) and elemental mapping using laser ablation (LA). The rapid collection of full elemental mass spectra promotes non-target approaches, fast imaging as well as inquiries of particle composition. However, one shortcoming often associated with ICP-ToF-MS is a lack of detection power due to lower duty cycles relative to sequentially operating mass analysers targeting only a limited number of elements. The sensitivity of ICP-ToF-MS can be increased using two strategies, which are detailed in this study. First, instead of analysing full mass spectra, elements in the low and high mass ranges were excluded from analysis using a Bradbury–Nielsen gate. The resulting restricted mass range was acquired up to 5 times faster increasing duty cycles and sensitivity accordingly. Second, isotopes of polyisotopic elements recorded simultaneously were accumulated to increase signal to noise ratios. In a proof of concept, we applied SP ICP-ToF-MS for the first time to characterise upconversion nanoparticles (UCNPs) that contained Gd and Yb. Both signal amplification strategies were combined and the consequences for detection limits and signal to noise ratios were considered and compared to a standard method. Sensitivities were increased up to factor 27 when accumulating all Gd and Yb isotopes at 177 kHz, and size detection limits decreased by a factor of approximately 3. Improved figures of merit promoted more accurate investigations of UCNPs, which were characterised regarding size distributions and composition. As a second application, we demonstrated the utility of the described strategies in LA-ICP-ToF-MS. Mo and Se were targeted as relatively rare elements in rat brain tissue. Increased acquisition frequencies of 180 kHz and isotope accumulation resulted in drastically improved signal to noise ratios and enabled the mapping of both elements while still considering relevant neuroanatomical elements such as Fe and Zn.

Received 23rd August 2023
Accepted 27th November 2023

DOI: 10.1039/d3ja00288h

rsc.li/jaas

Introduction

Inductively coupled plasma mass spectrometry (ICP-MS) has become the method of choice for the characterisation of trace elements. New applications and technology have been developed and expanded the capabilities of ICP-MS vastly since its inception.[1,2] Following its commercial introduction in 1983,[3] solid sampling,[4] bioimaging[5] and speciation analysis[6] were established by hyphenating ICP-MS with laser ablation (LA) and chromatography.[7,8] For the former, a pulsed laser is used to raster over a solid specimen and the ablated material is transported as dry aerosol for elemental analysis *via* ICP-MS. In conjunction with adequate soft- and hardware, LA-ICP-MS is capable of reconstructing the two-dimensional distribution of trace elements.[7] ICP-MS can further be employed to characterise particle dispersions using an approach pioneered by Degueldre in 2003 known as single particle (SP) ICP-MS.[9] Here, nanoparticles (NPs) are introduced individually into the plasma and following the generation of elemental cations, a spatially separated ion cloud can be extracted for each particle for mass spectrometry. The operation of rapid mass analysers enables the probing of each ion cloud with several data points and to count and characterise individual NP signal pulses. This provides the means to construct models on particle number concentrations (PNCs) and mass/size distributions.[10]

Technological advances such as the introduction of the collision reaction cell (CRC),[11] sector field analysers[12] and tandem mass spectrometry[13,14] redefined the figures of merit for ICP-MS and enabled new applications. Despite early efforts, the development of time-of-flight (ToF)-based mass spectrometry was initially hampered due to the noisy ICP ion source, the high abundance of Ar^+ ions, low duty cycles and mass bias effects.[15,16] However, improvements in instrumentation made within the last twenty years have enabled modern ICP-ToF-MS instruments

[a]*Hyphenated Mass Spectrometry Lab, University of Technology Sydney, NSW, Australia*
[b]*Institute of Chemistry, University of Graz, Austria. E-mail: David.Clases@uni-graz.at*
[c]*School of Biomedical Engineering, Faculty of Engineering and Information Technology, University of Technology Sydney, NSW, Australia*
[d]*Nu Instruments, Wrexham, UK*

to set new benchmarks in multi-elemental imaging and the analysis of individual particles. Although sensitivity is lower when compared against quadrupole-based ICP-MS (ICP-QMS), ICP-ToF-MS has the crucial advantage to acquire full elemental mass spectra rapidly (at rates exceeding 35 kHz) and save binned mass spectra continuously at rates exceeding 10 kHz.[17,18] This capability promotes both the multi-elemental characterisation of individual particles *via* SP analysis as well as the rapid mapping of elemental distributions in micro-scaled structures *via* LA analysis. For the latter, fast washout systems are typically installed to promote rapid aerosol introduction and enable the transient resolution of individual laser pulses.[19] While these systems are the basis for fast imaging and increase signal to noise ratios (SNRs), they limit the maximum number of analysable isotopes when applying sequentially operating mass analysers such as quadrupoles.[20,21] The extraction of ablated aerosol plumes typically occurs in the lower millisecond range, which means that only a handful of elements can be monitored with ICP-QMS performing *m*/*z* scanning operations on a similar time scale. The case is different when using LA-ICP-ToF-MS, which records all elements simultaneously and therefore enables full elemental analysis of the aerosol plume from each laser shot.[17] The rapid acquisition of full mass spectra is also a critical advantage for the characterisation of individual NPs in single particle mode. Here, quadrupoles are too slow to analyse individual ion clouds for different isotopes/elements and therefore, only one element per particle is detectable using SP ICP-QMS. This limits both the non-target analysis of particles in unknown samples and the inquiry of particle compositions severely.[22–25]

Both SP and LA-ICP-ToF-MS have set a new paradigm for the characterisation of elemental distributions and compositions on the micro- and nanoscale. More comprehensive investigations into the interplay and associations between different elements in discrete structures are now possible. However, when compared against ICP-QMS, ICP-ToF-MS lacks sensitivity, preventing some applications such as the characterisation of small and/or heterogeneous NPs or the analysis of trace entities at high resolutions *via* LA-ICP-MS. This study demonstrates two strategies to optimise ICP-ToF-MS duty cycles and to increase sensitivity. These strategies were applied to characterise upconversion nanoparticles (UCNPs) and to map essential low level trace elements in rat brain tissue.

Materials and methods

Instrumentation

A Vitesse ICP-ToF-MS system by Nu Instruments (Wrexham, UK) was operated at varying acquisition frequencies ranging from 35 to 180 kHz. The plasma was operated at 1.4 kW and the segmented reaction cell was operated with He and H_2 flow rates between 5 and 12 mL min^{-1}. The typical nebuliser flow rate was approximately 1.35 L min^{-1}. For SP experiments, binned spectra were written to disc at frequencies between 10 and 12.5 kHz, and for LA experiments at 1 kHz. The LA system was an Analyte G2 excimer system (193 nm; Teledyne Photon Machines, Omaha, US) equipped with an aerosol rapid introduction system (ARIS; Teledyne Photon Machines) achieving wash out times of 15 ms. The laser was operated at 1 J cm^{-2} and rastered at 250 Hz using a 35 μm square and a scan speed of 2187.5 μm s^{-1}. The LA-ICP-ToF-MS set-up was tuned analysing a 612 NIST "Trace Elements in Glass" standard. For SP analysis, the ICP-ToF-MS system was equipped with a concentric nebulizer (Weilburg, Germany, Glass Expansion) and a cyclonic spray chamber. Transport efficiency was 1.7% and was determined by analysing Au NPs (nanoComposix, US) and ionic standards with a known mass and concentration, respectively, using an automated approach *via* the SP data processing platform SPCal.[26]

Software and data processing

For LA-ICP-ToF-MS analyses, data acquisition was performed using Nu Codaq software (Nu Instruments). For elemental mapping, Nu Quant (Nu Instruments) was used to export mass spectra which were further processed using Pew^2 software by Lockwood *et al.*[27] For Mo, the isotopes ^{95}Mo, ^{97}Mo, ^{98}Mo and ^{100}Mo were accumulated and their sum was abbreviated with ΣMo. For Se, the isotopes ^{78}Se, ^{80}Se and ^{82}Se were accumulated to form ΣSe. For the calculation of SNRs, noise was determined as standard deviation of the gas blank and used as a divisor for the signal in each pixel. For comparisons, ΣSe and ΣMo were overlaid with maps of ^{56}Fe and ^{64}Zn to visualize neuroanatomy.

SP ICP-ToF-MS raw data was analysed using SPCal developed by Lockwood *et al.*[26] and adapted for ICP-ToF-MS data structure. Decision limits were determined using compound Poisson sampling of a lognormal approximation of the signal ion distribution.[24,28] Briefly, for each value k of the probability mass function of the expected background, the sum of k lognormal distributions was computed. The cumulative density function (CDF) of each lognormal was then calculated, weighted by the Poisson probability of k and summed. The decision limit was then determined as the first value above the desired zero-truncated quantile, using the summed CDF. Here, an α value of 10^{-6} was used to determine a decision limit, which means that from 10^6 detection intervals, only one false detection of a particle would be expected. The interested reader will find more information elsewhere.[24] Contiguous regions above the mean signal were accumulated for mass and size calibration. Signals from different elements detected coincidently were considered for modelling single particle composition. Three sums of isotopes were compared against the analysis of individual isotopes: ΣYb accumulating all Yb isotopes, ΣGd accumulating all Gd isotopes, and ΣYb + ΣGd accumulating all Gd and all Yb isotopes.

Consumables and samples

Elemental standards at 1000 μg L^{-1} for ICP-MS (Single-Element ICP-Standard-Solution Roti®Star) were diluted to working conditions using ultra-pure water (18.2 MΩ cm; Merck Millipore, Bedford, USA). An 80 nm Au NP standard was obtained from nanoComposix (San Diego, US). Dilutions were performed in tubes made of polypropylene.

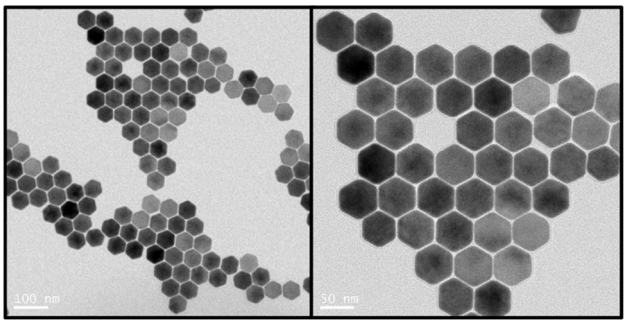

Fig. 1 TEM images of UCNPs with hexagonal shape and average size of 54.6 nm.

A rat brain cryosection with a thickness of 30 μm was air dried at room temperature. To avoid the washout of endogenous elements, no further treatments were applied.

UCNPs samples were manufactured following previous reports by Liu *et al.*[29,30] 1 mmol (in total) lanthanide chlorides ($GdCl_3$, $YbCl_3$ and $ErCl_3$) were dissolved in methanol base at a molar ratio of 50 : 49 : 1 and then mixed with 6 mL oleic acid and 15 mL octadecene. The methanol was evaporated completely during the heating process and the mixture was kept at 150 °C for 0.5 h. The solution was then cooled to room temperature (RT) and spiked with 10 mL methanol solution containing 4 mmol NaOH and 2.5 mmol NH_4F was added and stirred for 0.5 h at RT. The mixture was heated up again to 90 °C and kept for 0.5 h and then further heated to 150 °C and kept for 10 minutes to evaporate the methanol completely. Finally, the solution was heated and kept at 300 °C for 1.5 h. The size of the UCNPs was tailored by controlling the heating rate. The UCNPs were washed three times using a mixed solution of oleic acid, cyclohexane, methanol and ethanol after the reaction solution was cooled to RT. The morphology of the UCNPs were characterised using Transmission Electron Microscopy (TEM, FEI Tecnai T20 Transmission Electron Microscope at 200 kV accelerating voltage) as shown in Fig. 1. UCNPs had a hexagonal shape and mean sizes were 54.6 nm. For SP ICP-ToF-MS, UCNPs were dispersed and diluted in water and directly analysed.

Results and discussion

Duty cycle and isotope accumulation

The ToF analyser samples only a fraction of ions extracted from the plasma. Ions in a push out region are accelerated orthogonally into the reflectron to equal kinetic energies and as such, different m/z travel at different velocities, which is the fundament for m/z calibration. The duty cycle of a ToF analyser is defined by the period it takes to complete the acquisition of a mass spectrum. When acquiring the complete mass range, considerable time is required before the next push out event can be triggered, which results in a relatively low fraction of ions analysed. While full mass ranges (5–250 amu) could be acquired at approximately 35 kHz, this speed was too fast for the processing units and spectra were therefore binned before writing data to disc at a maximum rate of approximately 12.5 kHz. The analysed mass range could be controlled using a Bradbury–Nielsen gate, further referred to as an "ion blanker". The blanker was situated between the push out region and the reflectron, and consisted of a set of wires that generate an electric field on demand when applying a current. The timely and repeated activation of the ion blanker restricted the acquired mass range by deflecting ions at specific time slots. The removal of m/z ranges on both sides of the mass spectrum enabled acquisitions of restricted mass regions at higher rates. Acquisition frequency was increased from 35 kHz (full mass spectra) to up to 177 kHz for SP ICP-ToF-MS applications and to up to 180 kHz for LA-ICP-ToF-MS applications. The reduction of the acquired mass range enabled accelerated ion push out, which translated into increasing duty cycles and improved sensitivity.

Sequentially operating mass analysers like quadrupoles can only analyse a fraction of a polyisotopic element at a time and recent studies focussed on improving SNRs by increasing the mass bandpass beyond 1 amu to transmit several isotopes simultaneously.[31] These 'increased bandpass' methods have been successfully applied to LA-ICP-MS,[32] SP ICP-MS[33] and LC-ICP-MS[34] to improve figures of merit. The simultaneous acquisition of various isotopes is an intrinsic feature of ICP-ToF-MS, and a similar strategy can be implemented using a facile post-analysis processing step, in which several isotopes are accumulated to analyse a higher fraction of a polyisotopic element. The possibility to select or omit certain isotopes provides control to avoid spectral interferences and using the higher resolution of the ToF analyser as well as tuning the collision/reaction cell facilitates the bypassing of polyatomic interferences.

The following sections describe both mentioned approaches in a practical setting. Duty cycles were increased using an ion blanker to acquire restricted spectra at up to 180 kHz and isotopes of the polyisotopic elements Se, Mo, Gd and Yb were accumulated in a post-analysis processing step to further enhance SNRs.

SP ICP-ToF-MS of UCNPs

Engineered NPs are an innovative driving force in various scientific disciplines and new materials are manufactured at increasing rates. One example are upconversion NPs (UCNPs), which have applications in diverse fields due to their unique optical, electronic, and magnetic properties. They consist of a host crystal (*e.g.*, $NaYF_4$ or $NaGdF_4$) that is doped with lanthanide ions to promote the consecutive absorption of low-energy photons and the subsequent photon upconversion. Fields of applications include high-resolution microscopy, biosensing, solar energy harvesting, optical bioimaging, drug delivery vehicles and multi-modal diagnostics.[35–39] The optical properties and nanophotonic behaviours of UCNPs highly depend on their size, structure, and stoichiometry and alas, a bottle neck for the development and application of UCNPs is the limited number of suitable analytical techniques to characterise these particles with sufficient detail. SP ICP-QMS was recently used to characterise UCNPs regarding their size and bulk composition.[33] However, ToF analysis provides additional

detail by analysing elemental composition on a single particle basis.

This study focussed on UCNPs containing Gd and Yb, which suggested to centre the investigated mass region around ^{152}Gd and ^{176}Yb as lightest and heaviest isotopes, respectively, to enhance duty cycle. However, applying a current to the ion blanker whilst acquiring small mass ranges created signal artefacts that required the expansion of the acquired mass range on the low mass end. The optimum size of the mass range (and therefore the optimum acquisition frequency) was investigated by evaluating background intensities for elements briefly after the blanking events. Background/noise levels were predicted for masses between 130 and 185 amu by recording the full spectra without blanking events ($I_{35\ \mathrm{kHz}}$) and factoring in the expected level of signal enhancement caused by higher duty cycles $\left(\frac{177\ \mathrm{kHz}}{35\ \mathrm{kHz}}\right)$. Respective values were compared against an experimental value ($I_{177\ \mathrm{kHz}}$) obtained when acquiring the isolated mass range at higher rates using the ion blanker, as described in eqn (1). Here, N signifies the level of background/noise and I were intensities recorded for a solution containing Yb and Gd at 35 and 177 kHz, respectively.

$$N = I_{35\ \mathrm{kHz}} \frac{177\ \mathrm{kHz}}{35\ \mathrm{kHz}} - I_{177\ \mathrm{kHz}} \quad (1)$$

Fig. 2 shows the noise level N over the acquired mass range, and it was evident that immediately after the blanking event (red), noise levels were significantly altered in a mass range from 130–147 amu, which corresponded to a time of approximately 1 μs (yellow). Only after this settling time did noise levels

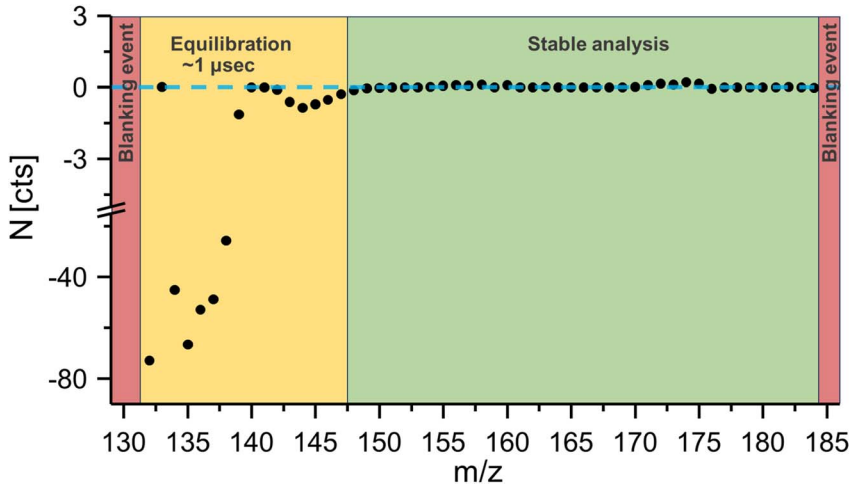

Fig. 2 The noise level following a blanking event was investigated. Theoretical background values were determined by analysing a full mass spectrum at 35 kHz and determined intensities were multiplied by the expected signal amplification factor when acquiring signal at 177 kHz. Theoretical values were compared against experimental values according to eqn (1). Blanking created signal artifacts for a period of approximately 1 μs.

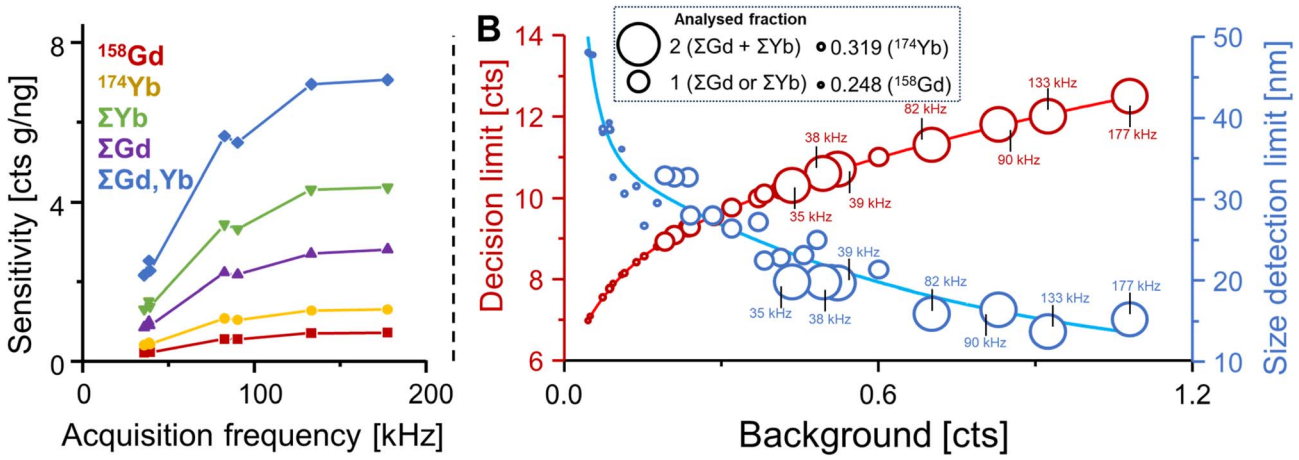

Fig. 3 (A) Shows the effects of isotope accumulation and increasing acquisition frequencies on sensitivity. (B) Compares the Compound Poisson decision limit (red), which increases when isotopes are accumulated at increasing acquisition rates. Despite increasing noise levels, enhanced size detection limits are achieved. The size of circles as individual data points corresponds to the isotope fraction analysed in a particle due to post-analysis accumulation.

return to baseline values. Consequently, when analysing isotopes with masses between 152 and 176 amu the low mass cut off was lowered to 130 amu to ensure the absence of ion blanker induced signal artifacts in the mass regions of interest.

Fig. 3A considers the most abundant isotopes of Gd (^{158}Gd) and Yb (^{174}Yb) and demonstrates how sensitivities were increased when accelerating acquisition frequency. Sensitivities for ^{158}Gd and ^{174}Yb increased by a factor of approximately 3.2 from 0.215 and 0.407 counts per g ng^{-1} to 0.69 and 1.25 counts per g ng^{-1}, respectively, and size detection limits decreased from 38.6 to 29.5 nm.

The simultaneous consideration of all isotopes of an element increased sensitivities by an additional factor of 3.9 (Gd) and 3.3 (Yb). The combination of increased acquisition frequency and the detection of various isotopes increased sensitivity drastically to 2.7 and 4.2 counts per g ng^{-1} for Gd and Yb, respectively. Given that Yb and Gd were always detected coincidently suggested the joint acquisition of both Gd and Yb isotopes resulting in additional improvements of up to 6.8 counts per g ng^{-1} at 177 kHz, which corresponded to a 32-fold increase when compared to ^{158}Gd alone. Both increasing the acquisition frequency and accumulating signals from different isotopes increased noise levels. In SP ICP-ToF-MS, noise levels are dependent on the background signal and can be modelled with compound Poisson statistics.[24,28] To compare the association between noise, background and figures of merit, the decision limit was used as proxy for noise and plotted (red) together with experimental size detection limit (blue) against measured background levels in Fig. 3B. The acquired fraction of isotopes per particle is reflected in the size of data points: the largest circles represent the accumulation of all Yb and all Gd isotopes, the second largest circles represent the accumulation of all isotopes for either Gd or Yb, individually, and smaller circles signify the analysis of individual isotopes. For the highest signal accumulation, acquisition frequencies are also listed. It was apparent that larger analysed fractions and faster acquisition rates increased background values and therefore the decision limit. However, resulting size detection limits for an UCNP ($NaGd_{0.5}Yb_{0.5}F_4$) were still improved due to the sensitivity increasing significantly faster relative to the noise. In summary, size detection limits decreased substantially with increasing acquisition speed and when analysing isotopes jointly. Specifically, size detection limits decreased from 47.7 and 38.5 nm for ^{158}Gd and ^{174}Yd, respectively, to 25 and 21.3 nm when acquiring ΣYb and ΣGd. The joint acquisition of both Yb and Gd isotopes (ΣYb + ΣGd at 177 kHz) decreased the limit further to 15.2 nm.

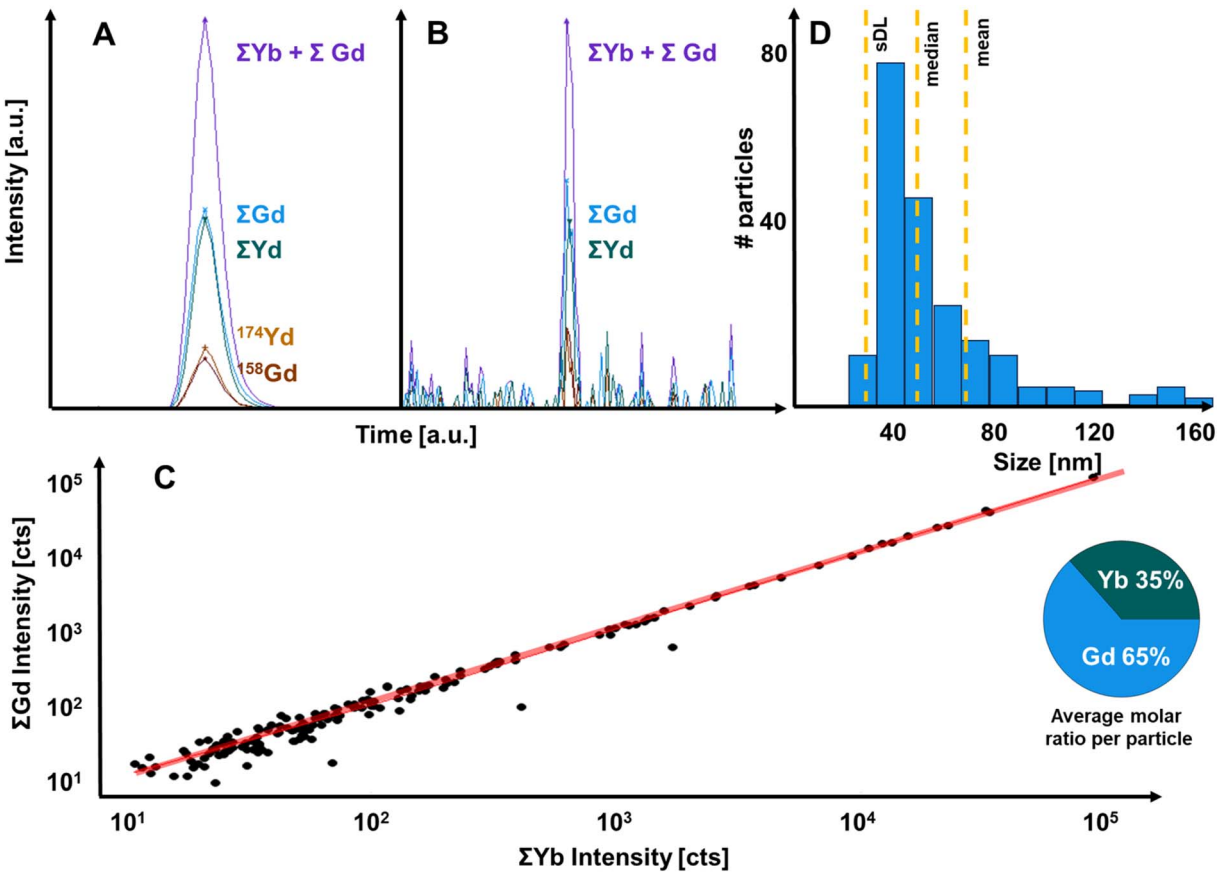

Fig. 4 (A) and (B) Show a transient signal acquisition of an UCNP. The two most abundant isotopes of Gd and Yb are indicated and compared against the signal resulting from isotope accumulation. (C) Shows the linear association between Yb and Gd on a single particle basis, which was used to determine the average molar composition of single particles. (D) shows the size distribution, which was determined using the previously determined stoichiometry.

The increased limits of analysis enabled the characterisation of single UCNPs as demonstrated in Fig. 4. Fig. 4A shows the detection of one UCNP signal containing signals from Gd and Yb isotopes. It is evident that post-analysis isotope accumulation increased signal drastically. Fig. 4B shows the effect of isotope accumulation for a small UCNP. Here, signals for ^{174}Yb and ^{158}Gd were below the decision limit, and the particle was only detected based on the joint consideration of lanthanide isotopes. The comparison of accumulated signal fractions in individual particles is plotted in Fig. 4C and demonstrated a consistent stoichiometry across detected particles and a mean molar ratio of 1.86 Gd:Yb was determined on a single particle basis. Fig. 4D shows the size distribution which considered the determined elemental composition of particles. When measuring single particle composition, the impact of interferences needs to be considered. For example, Gd isotopes may form oxides which interfere with Yb isotope signals (*e.g.*, ^{156}Gd^{16}O would interfere with ^{172}Yb) and therefore lead to systematic errors. This could be mitigated by controlling the oxide formation rate during the tuning process as well as by the operation of relatively high He and H_2 gas flows in the collision/reaction cell. The impact of interferences was investigated by comparing experimental and natural isotopic abundances. In this case, the experimental ratios for ^{174}Yb/^{172}Yb and ^{157}Gd/^{156}Gd in single particles deviated only by approximately 1% from theoretical values demonstrating that interferences did not play a significant role.

LA-ICP-ToF-MS for bioimaging

The strategies to increase acquisition frequency and to accumulate isotopes *via* post-analysis processing were also applicable in LA-ICP-ToF-MS and improved the mapping of elements by increasing SNRs. The spatial resolution of LA-based mapping is primarily associated with SNRs and options to increase these are in high demand to promote more sensitive trace analyses as well as higher resolution mapping. In a proof of principle, this study focused on the analysis of Se and Mo as two essential trace elements with low abundance in rat brain. For comparison, one brain hemisphere was analysed at 180 kHz (m/z 56–100) accumulating selected isotopes of Se and Mo, and the other hemisphere was analysed at 35.5 kHz (m/z 5–250) targeting only the most abundant isotopes, ^{80}Se and ^{98}Mo. The selection of isotopes for signal accumulation needs to consider interferences. In this case, polyatomic interferences were limited through the use of the collision/reaction cell, enabling the analysis of isotopes such as ^{78}Se and ^{80}Se. However, the glass support for the tissue was found to contain traces of elements (*e.g.*, Zr and Ge) which have spectral overlaps with Mo and Se. To maximise contrast and SNRs, affected isotopes were omitted from accumulation and only entities improving figures of merit were exploited. For this application, ΣSe and ΣMo considered ^{78}Se, ^{80}Se and ^{82}Se as well as ^{95}Mo, ^{97}Mo, ^{98}Mo and ^{100}Mo, respectively. Fig. 5A and B show the SNRs for ΣSe and the most abundant isotope, ^{80}Se, at 180 kHz and 35.5 kHz, respectively. Both increased acquisition frequency as well as isotope accumulation improved SNRs and enabled the mapping of Se in brain tissues with sufficient contrast. The same approach was applied for the mapping of Mo and is shown in Fig. 5C and D. As before, significantly improved SNRs were obtained when accumulating Mo isotopes and increasing acquisition frequency. In summary, isotope accumulation and higher acquisition frequency improved SNRs and enabled the mapping of Se and Mo at 35 μm spatial resolution in brain tissues. The described strategies have a high utility to be applied in conjunction with the multi-elemental capabilities of ToF. Although increasing duty cycles are inherent with decreasing mass ranges, acquisition frequencies and mass windows can be tuned to include relevant entities. In this example, a mass range of 56 to 100 amu was chosen to enable the coincidental mapping of Mn, Fe, Cu, Zn, Co and other relevant elements in addition to Se and Mo isotopes. An example is shown Fig. 5E and F which demonstrates the joint analysis of Se (Fig. 5E) and Mo (Fig. 5F) with Fe

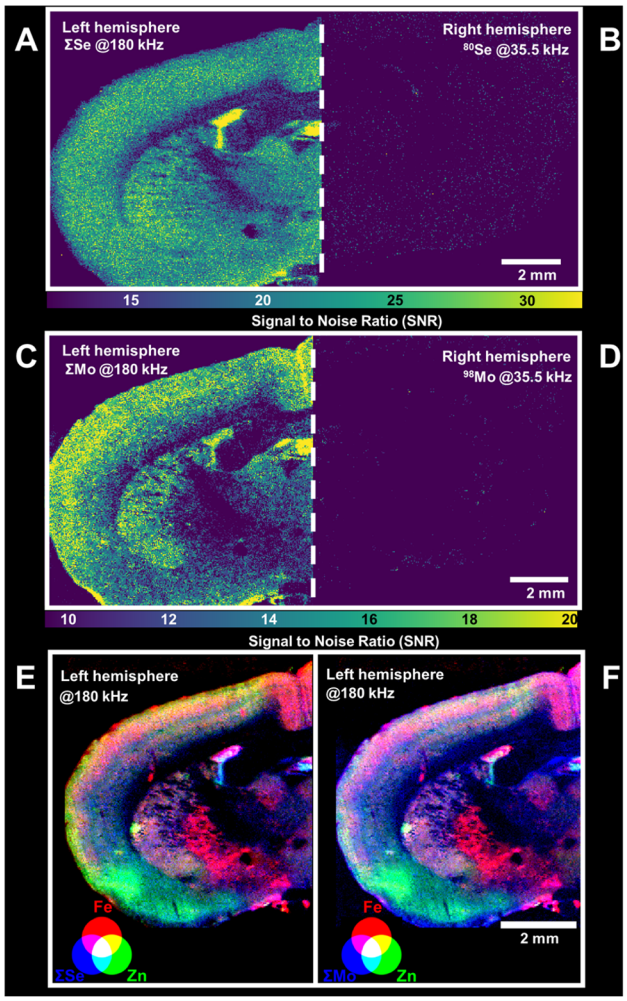

Fig. 5 Isotope accumulation and increased acquisition frequencies were applied to element mapping *via* LA-ICP-ToF-MS. (A) Shows the distribution of Se isotopes at 180 kHz in the left hemisphere of a rat brain and (B) shows the distribution of ^{80}Se in the right hemisphere of the same brain recorded at 35.5 kHz. (C) and (D) Show the same set up for the analysis of ΣMo and ^{98}Mo. Despite reduced mass ranges, Fe and Zn could be mapped simultaneously and enabled correlative studies as shown in (E) and (F).

and Zn as two neurologically relevant entities. It was apparent that the simultaneous analysis of Se and Mo with Zn and Fe enabled a correlative analysis as well as the resolution of neurological anatomy and fine structures.

Conclusions

ICP-ToF-MS offers conspicuous advantages for the mapping of elements and the characterisation of individual particles. However, a lack of sensitivity may be a pitfall for certain applications, such as when trace elements are acquired with high resolution in LA analysis or when small and heterogenous nanoparticles are to be characterised *via* SP analysis. Here we described two strategies that can be applied to increase sensitivity and push the limits of analysis. First, restricting mass spectra to critical mass ranges using an ion blanker increased the acquisition frequency, which enhanced duty cycles and sensitivity. Second, for polyisotopic elements, simultaneously acquired isotopes could be accumulated in a post-analysis approach to consider larger element fractions. However, confounding interferences needed to be taken into account to maximise SNRs ratios.

These strategies are simple to implement and were demonstrated for the analysis of individual UCNPs *via* SP ICP-ToF-MS and for the mapping of Se and Mo in rat brain *via* LA-ICP-ToF-MS. While increasing sensitivities are accompanied with growing levels of noise, overall SNRs increased drastically and reduced detection limits. The described strategies are universally applicable to enhance limits of analysis and can be considered for high resolution mapping applications as well as the analysis of small and heterogenous NPs.

Conflicts of interest

L. S. works for Nu Instruments.

Acknowledgements

The authors acknowledge the financial support by the University of Graz.

References

1 D. Clases and R. Gonzalez de Vega, Facets of ICP-MS and their potential in the medical sciences—part 1: fundamentals, stand-alone and hyphenated techniques, *Anal. Bioanal. Chem.*, 2022, **414**(25), 7337–7361, DOI: 10.1007/s00216-022-04259-1.

2 D. Clases and R. Gonzalez de Vega, Facets of ICP-MS and their potential in the medical sciences—part 2: nanomedicine, immunochemistry, mass cytometry, and bioassays, *Anal. Bioanal. Chem.*, 2022, **414**(25), 7363–7386, DOI: 10.1007/s00216-022-04260-8.

3 A. L. Gray, The evolution of the ICP as an ion source for mass spectrometry, *J. Anal. At. Spectrom.*, 1986, **1**(6), 403–405.

4 A. L. Gray, Solid sample introduction by laser ablation for inductively coupled plasma source mass spectrometry, *Analyst*, 1985, **110**(5), 551–556, DOI: 10.1039/AN9851000551.

5 S. Wang, R. Brown and D. J. Gray, Application of Laser Ablation-ICPMS to the Spatially Resolved Micro-Analysis of Biological Tissue, *Appl. Spectrosc.*, 1994, **48**(11), 1321–1325, DOI: 10.1366/0003702944028001.

6 J. J. Thompson and R. S. Houk, Inductively Coupled Plasma Mass Spectrometric Detection for Multielement Flow Injection Analysis and Elemental Speciation by Reversed-Phase Liquid Chromatography, *Anal. Chem.*, 1986, **58**(12), 2541–2548.

7 P. A. Doble, R. G. de Vega, D. P. Bishop, D. J. Hare and D. Clases, Laser ablation-inductively coupled plasma-mass spectrometry imaging in biology, *Chem. Rev.*, 2021, **121**(19), 11769–11822.

8 D. P. Bishop, D. J. Hare, D. Clases and P. A. Doble, Applications of liquid chromatography-inductively coupled plasma-mass spectrometry in the biosciences: a tutorial review and recent developments, *Trends Anal. Chem.*, 2018, **104**, 11–21.

9 C. Degueldre and P.-Y. Favarger, Colloid analysis by single particle inductively coupled plasma-mass spectroscopy: a feasibility study, *Colloids Surf., A*, 2003, **217**(1), 137–142, https://www.sciencedirect.com/science/article/pii/S092777570200568X.

10 B. Meermann and V. Nischwitz, ICP-MS for the analysis at the nanoscale – a tutorial review, *J. Anal. At. Spectrom.*, 2018, **33**(9), 1432–1468, http://xlink.rsc.org/?DOI=C8JA00037A.

11 S. D. Tanner, V. I. Baranov and D. R. Bandura, Reaction cells and collision cells for ICP-MS: a tutorial review, *Spectrochim. Acta, Part B*, 2002, **57**, 1361–1452.

12 U. Gießmann and U. Greb, High resolution ICP-MS - a new concept for elemental mass spectrometry, *Fresenius. J. Anal. Chem.*, 1994, **350**(4–5), 186–193.

13 D. P. Bishop, D. Clases, F. Fryer, E. Williams, S. Wilkins, D. J. Hare, *et al.*, Elemental bio-imaging using laser ablation-triple quadrupole-ICP-MS, *J. Anal. At. Spectrom.*, 2016, **31**, 197–202.

14 E. Bolea-Fernandez, L. Balcaen, M. Resano and F. Vanhaecke, Overcoming spectral overlap: via inductively coupled plasma-tandem mass spectrometry (ICP-MS/MS). A tutorial review, *J. Anal. At. Spectrom.*, 2017, **32**, 1660–1679.

15 D. P. Myers and G. M. Hieftje, Preliminary Design Considerations and Characteristics of an Inductively Coupled Plasma-Time-of-Flight Mass Spectrometer, *Microchem. J.*, 1993, **48**(3), 259–277, https://www.sciencedirect.com/science/article/pii/S0026265X83711021.

16 D. P. Myers, G. Li, P. Yang and G. M. Hieftje, An inductively coupled plasma-time-of-flight mass spectrometer for elemental analysis. Part I: optimization and characteristics, *J. Am. Soc. Mass Spectrom.*, 1994, **5**(11), 1008–1016.

17 C. J. Greenhalgh, O. M. Voloaca, P. Shaw, A. Donard, L. M. Cole, M. R. Clench, *et al.*, Needles in haystacks: using fast-response LA chambers and ICP-TOF-MS to

identify asbestos fibres in malignant mesothelioma models, *J. Anal. At. Spectrom.*, 2020, **35**(10), 2231–2238, DOI: **10.1039/D0JA00268B**.

18 A. Azimzada, I. Jreije, M. Hadioui, P. Shaw, J. M. Farner and K. J. Wilkinson, Quantification and Characterization of Ti-, Ce-, and Ag-Nanoparticles in Global Surface Waters and Precipitation, *Environ. Sci. Technol.*, 2021, **55**(14), 9836–9844, DOI: **10.1021/acs.est.1c00488**.

19 S. J. M. Van Malderen, J. T. van Elteren and F. Vanhaecke, Development of a fast laser ablation-inductively coupled plasma-mass spectrometry cell for sub-μm scanning of layered materials, *J. Anal. At. Spectrom.*, 2015, **30**(1), 119–125, DOI: **10.1039/C4JA00137K**.

20 J. T. van Elteren, V. S. Šelih, M. Šala, S. J. M. Van Malderen and F. Vanhaecke, Imaging Artifacts in Continuous Scanning 2D LA-ICPMS Imaging Due to Nonsynchronization Issues, *Anal. Chem.*, 2018, **90**(4), 2896–2901, DOI: **10.1021/acs.analchem.7b05134**.

21 J. T. van Elteren, V. S. Šelih and M. Šala, Insights into the selection of 2D LA-ICP-MS (multi)elemental mapping conditions, *J. Anal. At. Spectrom.*, 2019, **34**(9), 1919–1931, DOI: **10.1039/C9JA00166B**.

22 A. Azimzada, J. M. Farner, I. Jreije, M. Hadioui, C. Liu-Kang, N. Tufenkji, *et al.*, Single- and Multi-Element Quantification and Characterization of TiO_2 Nanoparticles Released From Outdoor Stains and Paints, *Front. Environ. Sci.*, 2020, **8**, 91.

23 M. Tharaud, L. Schlatt, P. Shaw and M. F. Benedetti, Nanoparticle identification using single particle ICP-ToF-MS acquisition coupled to cluster analysis. From engineered to natural nanoparticles, *J. Anal. At. Spectrom.*, 2022, **37**(10), 2042–2052, DOI: **10.1039/D2JA00116K**.

24 R. Gonzalez de Vega, T. E. Lockwood, L. Paton, L. Schlatt and D. Clases, Non-target analysis and characterisation of nanoparticles in spirits via single particle ICP-TOF-MS, *J. Anal. At. Spectrom.*, 2023, **38**, 2656–2663.

25 R. Gonzalez de Vega, T. E. Lockwood, X. Xu, C. Gonzalez de Vega, J. Scholz, M. Horstmann, *et al.*, Analysis of Ti- and Pb-based particles in the aqueous environment of Melbourne (Australia) via single particle ICP-MS, *Anal. Bioanal. Chem.*, 2022, **414**, 5671–5681.

26 T. E. Lockwood, R. de Vega and D. Clases, An interactive Python-based data processing platform for single particle and single cell ICP-MS, *J. Anal. At. Spectrom.*, 2021, **36**(11), 2536–2544, DOI: **10.1039/D1JA00297J**.

27 T. E. Lockwood, M. T. Westerhausen and P. A. Doble, Pew(2): Open-Source Imaging Software for Laser Ablation-Inductively Coupled Plasma-Mass Spectrometry, *Anal. Chem.*, 2021, **93**(30), 10418–10423.

28 A. Gundlach-Graham, L. Hendriks, K. Mehrabi and D. Günther, Monte Carlo Simulation of Low-Count Signals in Time-of-Flight Mass Spectrometry and Its Application to Single-Particle Detection, *Anal. Chem.*, 2018, **90**(20), 11847–11855, DOI: **10.1021/acs.analchem.8b01551**.

29 D. Liu, X. Xu, Y. Du, X. Qin, Y. Zhang, C. Ma, *et al.*, Three-dimensional controlled growth of monodisperse sub-50 nm heterogeneous nanocrystals, *Nat. Commun.*, 2016, **7**(1), 10254, DOI: **10.1038/ncomms10254**.

30 D. Liu, X. Xu, F. Wang, J. Zhou, C. Mi, L. Zhang, *et al.*, Emission stability and reversibility of upconversion nanocrystals, *J. Mater. Chem. C*, 2016, **4**(39), 9227–9234, DOI: **10.1039/C6TC02990F**.

31 D. Clases, Swimming against the current – sacrificing unit mass resolution in ICP-MS to improve figures of merit, *J. Anal. At. Spectrom.*, 2023, **38**, 2518–2527.

32 D. Clases, R. Gonzalez de Vega, S. Funke, T. E. Lockwood, M. Westerhausen, R. V. Taudte, *et al.*, Matching sensitivity to abundance: high resolution immuno-mass spectrometry imaging of lanthanide labels and endogenous elements in the murine brain, *J. Anal. At. Spectrom.*, 2020, **35**, 728–735.

33 S. Meyer, R. Gonzalez de Vega, X. Xu, Z. Du, P. A. Doble and D. Clases, Characterization of Upconversion Nanoparticles by Single-Particle ICP-MS Employing a Quadrupole Mass Filter with Increased Bandpass, *Anal. Chem.*, 2020, **92**(22), 15007–15016, DOI: **10.1021/acs.analchem.0c02925**.

34 M. Horstmann, R. Gonzalez de Vega, D. P. Bishop, U. Karst, P. Doble and D. Clases, Determination of gadolinium MRI contrast agents in fresh and oceanic waters of Australia employing micro-solid phase extraction, HILIC-ICP-MS and bandpass mass filtering, *J. Anal. At. Spectrom.*, 2021, **36**, 767–775.

35 Z. Du, A. Gupta, C. Clarke, M. Cappadona, D. Clases, D. Liu, *et al.*, Porous Upconversion Nanostructures as Bimodal Biomedical Imaging Contrast Agents, *J. Phys. Chem. C*, 2020, **124**(22), 12168–12174.

36 Y. Liu, F. Wang, H. Lu, G. Fang, S. Wen, C. Chen, *et al.*, Super-Resolution Mapping of Single Nanoparticles inside Tumor Spheroids, *Small*, 2020, **16**(6), 1905572, DOI: **10.1002/smll.201905572**.

37 Q. Liu, Y. Sun, T. Yang, W. Feng, C. Li and F. Li, Sub-10 nm Hexagonal Lanthanide-Doped $NaLuF_4$ Upconversion Nanocrystals for Sensitive Bioimaging in Vivo, *J. Am. Chem. Soc.*, 2011, **133**(43), 17122–17125, DOI: **10.1021/ja207078s**.

38 C. Chen, L. Ding, B. Liu, Z. Du, Y. Liu, X. Di, *et al.*, Exploiting Dynamic Nonlinearity in Upconversion Nanoparticles for Super-Resolution Imaging, *Nano Lett.*, 2022, **22**(17), 7136–7143, DOI: **10.1021/acs.nanolett.2c02269**.

39 Y. Huang, Z. Du, G. Bao, G. Fang, M. Cappadona, L. McClements, *et al.*, Smart Drug-Delivery System of Upconversion Nanoparticles Coated with Mesoporous Silica for Controlled Release, *Pharmaceutics*, 2023, **15**(1), 89.

